Corrosion damage in WC-Co cemented carbides:

Residual strength assessment and 3D FIB-FESEM tomography characterization

J. M. Tarragó[1, 2], G. Fargas [1,2],E. Jimenez-Piqué[1,2], A. Felip [1], L. Isern[1], D. Coureaux[1], J.J.Roa[1,2], I. Al-Dawery[3] , J. Fair[3]and L. Llanes[1,2]

[1]CIEFMA ,Dept. deCiènciadelsMaterials i EnginyeriaMetal·lúrgica, UniversitatPolitècnica de Catalunya, Barcelona 08028, Spain

[2]CRnE, Centre de Recerca en Nanoenginyeria, UniversitatPolitècnica de Catalunya, Barcelona 08028, Spain

[3]Sandvik Hyperion, Coventry CV4 0XG, UK

Corresponding author e-mail: jose.maria.tarrago@upc.edu

Abstract

The effect of corrosion damage on cemented carbides was investigated. The study included residual strength assessment and detailed fractographic inspection of corroded specimens as well as detailed 3D FIB-FESEM tomography characterization. Experimental results point out a strong strength decrease associated with localized corrosion damage, i.e. corrosion pits acting as stress raisers, concentrated in the binder phase. These pits exhibit a variable and partial interconnectivity, as a function of depth from the surface, and are the result of heterogeneous dissolution of the metallic phase, specifically at the corrosion front. However, as corrosion advances the ratio between pit depth and thickness of damaged layer decreases. Thus, stress concentration effect ascribed to corrosion pits gets geometrically lessened, damage becomes effectively homogenized and relatively changes in residual strength as exposure time gets longer are found to be less pronounced.

Keywords: Corrosion, Cemented carbides, Residual strength, FIB Tomography

1. Introduction

Cemented carbides tools and components are commonly exposed to harsh working conditions that include a large variety of corrosive environments. Some examples of cemented carbide applications subjected to corrosion phenomena are: flow control components and wear tiles positioned on the flights of centrifuges used in chemical and petrochemical industry, metal forming tools, oil and gas inserts, and wood cutting inserts [1-5].

Literature on the corrosion behaviour of cemented carbides is relatively extensive (e.g. Refs. [6-19]). From these studies, several microstructural effects on corrosion response for these materials may be highlighted. First, in neutral and acidic solutions,corrosion in cemented carbides proceeds through selective binder leaching, whereas the WC particles are not much affected by the corrosion attack. This is not the case at alkaline pH, where the metallic binder passivates and WC shows active dissolution.Second, binder chemical nature has a large influence in the corrosion resistance of hardmetals. In this regard, it is known that addition of elements such as Cr, Ni, Mo or Ru in the Co binder phase generally enhances corrosion resistance. Third, grain size effects depend on the environment acidity, with microstructural refining yielding a beneficial effect on corrosion resistance under conditions in which the Co binder undergoes active/passive-transition.

Moreover, corrosion attack may also induce a detrimental effect on other critical performance-related parameters, such as wear resistance or mechanical strength. While there have been several studies addressed to evaluate the wear-corrosion interaction (e.g. Refs. [2-4,20-22], very few investigations havefocused on the influence of corrosion damage on the strength of hardmetals [1,12]. Such limitedinformation on strength-corrosion relationships for hardmetals is unfortunate from a structural integrity viewpoint, as it is relevant to find out how the limit state (defining failure) or the boundary between acceptable or unacceptable performance is affected by the damage induced by corrosion.

Understanding the influence of extrinsic damage (i.e. resulting from service-like conditions like occasional hard body impacts, continuous contact-related degradation, environmental assisted phenomena and/or thermal fluctuations) on mechanical strength requires a systematic and detailed characterization of the microstructural and micromechanical changes associated with it. Within this context, the advent of new and advanced characterization techniques had proven to be extremely helpful for achieving such holistic view. A clear example is the combined use of Field Emission Scanning Electron Microscopy (FESEM) and Focused Ion Beam (FIB) techniques for quantifying microstructure as well as evaluating tribological and damage phenomena in cemented carbides (e.g.Refs. [3,23-25]).

Following the above ideas, it is the purpose of the present work to assess the residual strength of a WC-Co hardmetal grade after inducing corrosion damage within the material. In doing so, mechanical testing is combined with fractographic analysis. Attempting to rationalize the found corrosion effects, the corresponding damage-microstructure interaction is finally characterized by means of 3D FIB-FESEM tomography. Final goal behind this investigation is to advance one more step on the proposal and validation of experimental and analytical protocols for assessment of effective structural integrity (i.e. reliability) of hardmetal tools and components on the basis of damage tolerance concepts.

2. Experimental procedure

The investigated material was an ultrafine-sized WC-Co hardmetal supplied by Sandvik Hyperion with high binder content. The key microstructural parameters: binder content ($\%_{wt}$ binder), mean grain size (d_{WC}), carbide contiguity (C_{WC}), and binder mean free path (λ_{binder}) are listed in Table 1. Mean grain size was measured following the linear intercept method, using FESEM micrographs taken in a JEOL-7001F unit. Carbide contiguity and binder mean free path were deduced from best-fit equations, attained after compilation and analysis of data published in the literature, on the basis of empirical relationships given by Roebuck and Almond [26] but extending them to include carbide size influence [27,28]. A minor amount of Cr_3C_2 was added to the composition as grain growth inhibitor.

Table 1. Nomenclature and microstructural parameters for the investigated cemented carbide.

Wt.% binder	d_{WC} (μm)	C_{WC}	λ_{binder} (μm)
15	0.47 ± 0.22	0.36 ± 0.02	0.24 ± 0.11

Mechanical characterization included hardness (HV30), flexural strength (σ_r) and fracture toughness (K_{Ic}). Hardness was measured using a Vickers diamond pyramidal indenter and applying a load of 294N. Strength and toughness testing was conducted using a four-point bending fully articulated test jig with inner and outer spans of 20 and 40 mm respectively. Flexural strength tests were performed on an Instron 8511 servohydraulic machine and at least 15 specimens of 45x4x3 mm dimensions were tested per grade. The surface which was later subjected to the maximum tensile loads was polished to mirror-like finish and the edges were chamfered to reduce their effect as stress raisers. Fracture toughness was determined using 45x10x5 mm single edge pre-cracked notch beam (SEPNB) specimens with a notch length-to-specimen width ratio of 0.3. Compressive cyclic loads were induced in the notched beams to nucleate a sharp crack and details may be found elsewhere [29]. Fracture toughness was determined by testing SEPNB specimens to failure at stress-intensity factor load rates of about 2 MPa$\sqrt{}$m/s.

Corrosion damage was induced in 45x4x3 mm beams by immersing them in an aerated synthetic mine water solution [9,30](pH = 6.7) whose composition is given in **Table 2**. Two sets of immersion tests were carried out in stagnant and stirred solution. Prior to immersion, the samples were polished and the edges chamfered following the same procedure used for flexural strength tests. Weight loss was measured after immersion tests performed at variable time, from 24 to 360h. The corrosion rate was determined according to equation (1):

$$\text{corrosion rate (mm/y)} = 87.6 * \left(\frac{w}{A\rho t}\right) \quad (1)$$

where w is the weight loss in mg; A is the surface area of the specimen in cm^2; ρ is the density of the material (13.93 g/cm^3); and t is the corrosion time in hours.

Residual flexural strength after corrosion was measured by testing the specimens to failure. At least 3 samples were tested per each corrosion time investigated in stirred solution. After failure, a detailed inspection of fracture surfaces was carried out by means of FESEM in order to identify failure sites.

Table 2. Synthetic mine water solution [30].

Compound	Concentration (mg/l)
$CaCl_2$	1038
Na_2SO_4	1237
$MgSO_4$	199
NaCl	1380

As it was referred above, one specific goal of this study is to document and understand corrosion damage in cemented carbides.Accordingly, a 3D tomography characterization of localized corrosion features (corresponding to 7 days – 168h – immersion time) was performed using the FIB-FESEM (Zeiss Neon 40)technique. In doing so, the corroded surface was initially examined to identify a region of interest of about 12x12 μm^2 for the image reconstruction (**Figure 1a**). Before sequential ion milling, a thin protective platinum layer was deposited on this area. Thus, a U-shaped trench with one cross-sectional surface perpendicular to the specimen surface was generated by FIB (**Figure 1b**). It permitted a correct visualization of the transversal section. Subsequently,corrosion damage-microstructure interaction was documented through series of FESEM micrographs obtained by periodical removal of a material. It was performed by millingthe U-shaped crater parallel to the cross-sectional surface, using the FIB's automated software. A volume of about 12x12x6μm^3 volume was ion milled and around 600 images were obtained for the reconstruction.

(a) 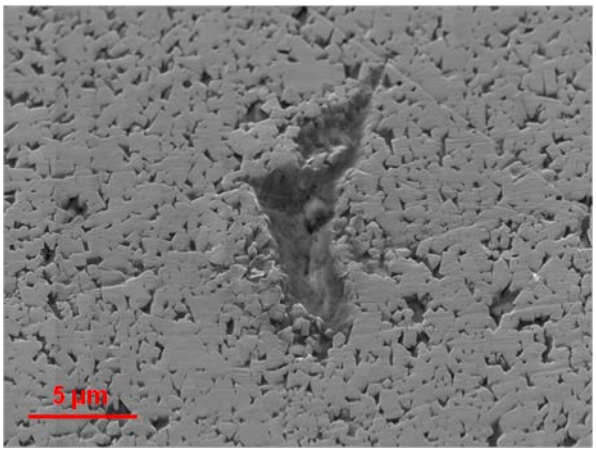

(b) 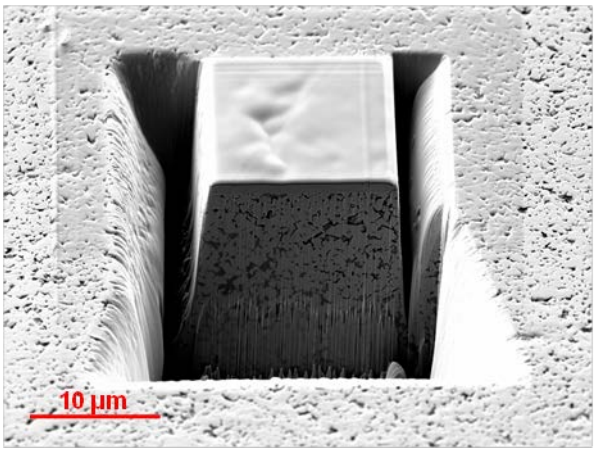

Figure 1.FESEM images corresponding to: (a) region of interest for 3D FIB-FESEM image reconstruction,and (b) U-trench generated by FIB around the regions of interest.

3. Results and discussion

3.1. Residual strength of corrosion-damagedhardmetals

Flexural strength and Weibull modulus, together with hardness and fracture toughness, for the investigated material are listed in **Table 3**. Such strength level is taken as reference condition in this study. The outstanding strength and Weibull modulusvalues are indicative of an optimal microstructure-processing-property relationship for this hardmetal grade which translates into high reliability (low variability) from a structural integrity viewpoint.

Table 3. Hardness, flexural strength, Weibull modulus and fracture toughness for the studied hardmetal.

HV30 (GPa)	Flexural strength (MPa)	Weibull modulus	K_{Ic} (MPa√m/s)
13.2 ± 0.1	3869 ± 109	42	11.3 ± 0.6

As it can be observed in Figure 2a, stirred solution yields higher weight loss compared to stagnant solution, the difference strongly increasingas immersion time gets longer. The corrosion rate for cemented carbide in stirred solution decreases with immersion time and starts to stabilize after 170 h approximately. However,even after 216h corrosion rate in agitated solution remains being at least twice that determined understagnant condition.

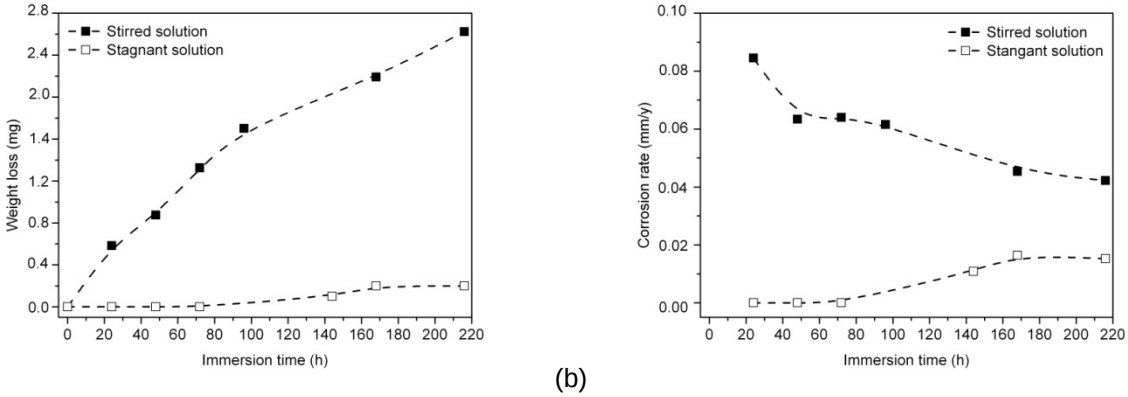

(a) (b)

Figure 2. Results after immersion tests in synthetic mine water solution: (a) Weight loss; (b) Corrosion rate.

One main objective of this study is to investigate how corrosion phenomena translate into effective damage. In this regard, strength testing not only provides a quantitative measure of the damage introduced by corrosion, but also yields critical information for assessing how well the corresponding microstructure may tolerate the introduced damage. Residual strength of the investigated cemented carbides is shown as a function of the corrosion time in **Figure 3a**. The results are normalised, with respect to strength data listed in **Table 3**, in **Figure 3b**.A relevant corrosion degradation effect on strength is discerned. It may be described as gradual and continuous, although exhibiting less pronounced relative changes, as exposure time increases. Strength drops are about 35% and 50% after 72h and 360h respectively. These results are in agreement with those found by Pugsley *et al.* [1] when studying the influence of tannic acid corrosion on the strength of hardmetal tools.

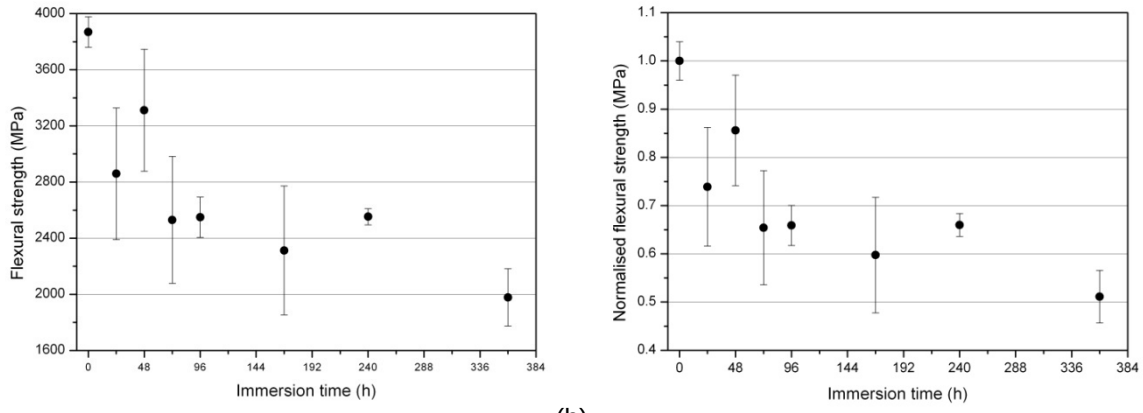

(a) (b)

Figure 3. Flexural strength (a) and normalised flexural strength (b) as a function of immersion time in the stirred solution corrosive media.

Aiming to document and understand damage-failure correlation, a detailed fractographicinspection was conducted by means of FESEM. Several observations may be done. First, failure sites were always associated with corrosion-induced damage, and examples are given in **Figure 4**. Second, as already reported, corrosion-induced damage is the result of preferential attack of the metallic binder [9-11,16]. As a

consequence, a WC skeleton surface layer is formed whose thickness increases as exposure time to mine water solution gets longer. Third, the referred WC skeleton layer does not grow deeper homogeneously; thus, corrosion pits are common features at the interface defining the corrosion front. Such localized corrosion features are quite relevant as they become the critical flaws in all the corroded specimens investigated (**Figure 4**). Such evidence is also concordant with the findings of Pugsley *et al.* [1], who rationalised the determined strength degradation on the basis of the stress concentration role played by the corrosion pits induced in the surface. Fourth, as corrosion damage evolves with exposure time, it should be noticed that ratio between pit depth and thickness of damaged layer decreases as corrosion front grows in a direction perpendicular to the surface. Accordingly, evolving damage (layer of WC skeleton) is somehow homogenized as exposure time increases, because stress concentration effect associated with localized pits gets geometrically lessened. Such ideas could then explain the trend described by the experimental data in **Figure 3** regarding lower relative changes in residual strength as exposure time increases.

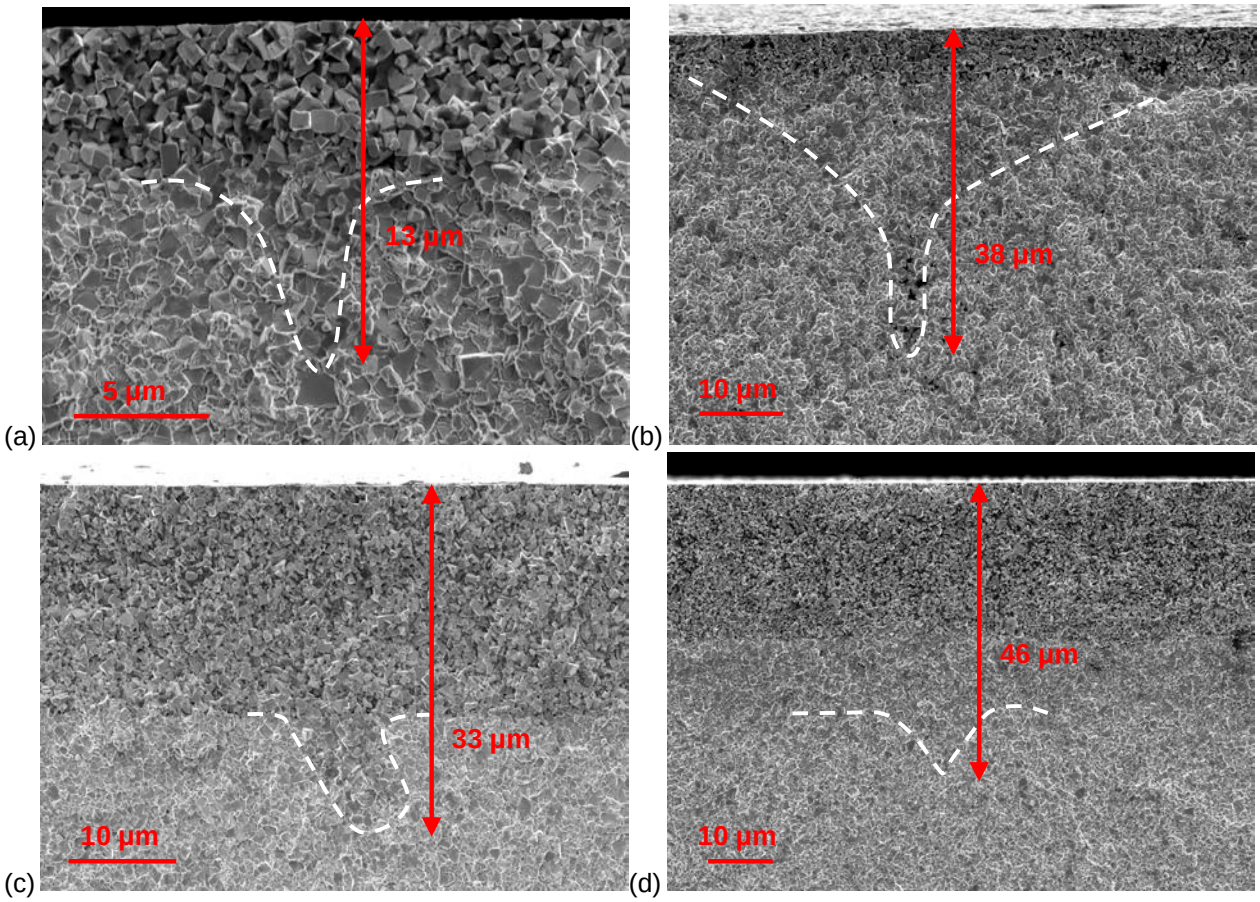

Figure 4. Critical corrosion damage that promotes failure for different corrosion times; (a) 24h, (b) 72h, (c) 168h and (d) 360h. Corrosion pits are marked with a white dotted line.

3.2. 3D FIB-FESEM tomography characterization of corrosion-induced damage

In the last few years fruitful examples on the suitability of the use of FIB-FESEM technique to characterize damage in cemented carbides have been presented (e.g. Refs.[3,22-25]). In this investigation, such an approach is followed to characterize corrosion damage-microstructure interactions in hardmetals. Hence, a 3D image reconstruction of the surface damage induced by corrosion after 168h was carried out. In **Figure 5,** two FESEM images corresponding to serial sections obtained during the FIB tomography procedureare presented. As it was already observed during the fractographicinspection, corrosion preferably takes place within the binder phase, leaving WC grains intact. However, corrosion is not completely homogeneous, regarding thickness of the damaged layer, with relative differences of up to 5µm being evidenced in the reconstruction. This figure also shows that microcracks appear within the corroded binder, probably due to formation of new cobalt phases [11,14]or cobalt dissolution and redeposition at small length scales [13].

Figure 5. Micrographs showing corrosion damage-microstructure interactions as imaged on serial sections obtained by means of FIB-FESEM tomography.

3D image reconstruction from the FIB-FESEM tomography data requires filtering, alignment and segmentation of theserial section images. In doing so, three different “phases” were identified corresponding to: carbides (yellow), binder (blue) and corrosion-induced microcracks (red). Additionally a microcrater, surface defect possibly generated due to chipping of locally exposed carbides, was reconstructed in green (**Figure 6**). The complete 3D reconstructed volume of the microstructure, containing the localized corrosion damage, is shown in **Figure 7**. For a better visualization of the 3D nature of both microstructure and damage, the three “phases” are also presented individually. As it was already discerned from 2D sliced images, the corrosion affected layer is not homogeneous in depth. As a consequence, potential stress raiser pits continuously develop at the corrosion front. This is evidenced by plotting the percentage of microcrackedbinder as a function of depth from the surface (**Figure 8**). It is clear from this graph that corrosion damage may be described as intrinsically heterogeneous (in terms of effective depth) at the corrosion front, but physically homogeneous regarding its interaction with microstructure, independent of the subsurface level. As a consequence, it evolves from microcrack nucleation associated with binder dissolution (from the center towards the carbide/binder interface [18]) to pronounced binder removal leaving an effectively unbound WC skeleton behind it. According to the data plotted in **Figure 8**, differences in amount of corroded binder between the WC skeleton layer and the heterogeneous corrosion front may be as large as 40%. Moreover, taking into consideration the damage scenario discerned in the fractographic inspection of broken corroded specimens (**Figure 4**), it could be speculated that length scale ahead of corrosion front where heterogeneity (corrosion pits) develops is rather independent (between 5 and 10 μm) of corrosion extension. Evaluation and understanding of this issue is beyond the scope of the present investigation, but additional research efforts will be devoted to it by the research group in the near future.

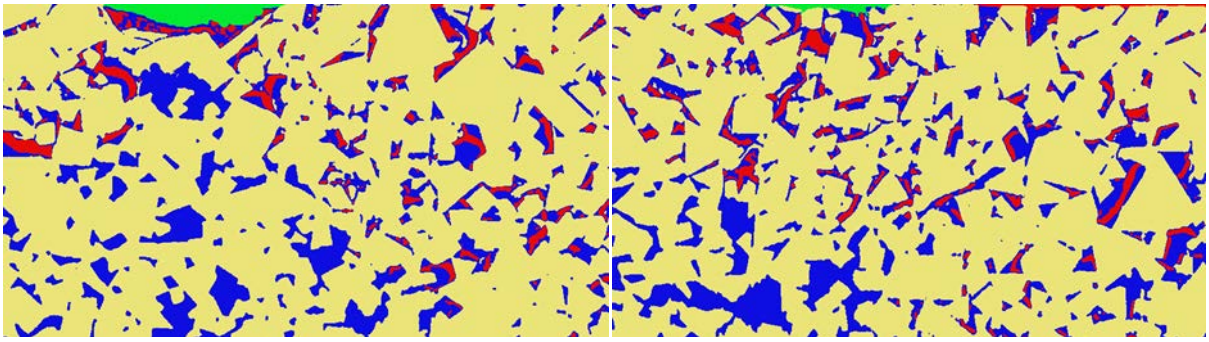

Figure 6. Filtered and segmented FESEM micrographs attained by FIB tomography.Three phases have been identified: WC carbides (yellow), metallic binder (blue), and corrosion-induced microcracks (red). Additionally, a surface microcrater (generated by chipping out of unbound carbides)is included in green.

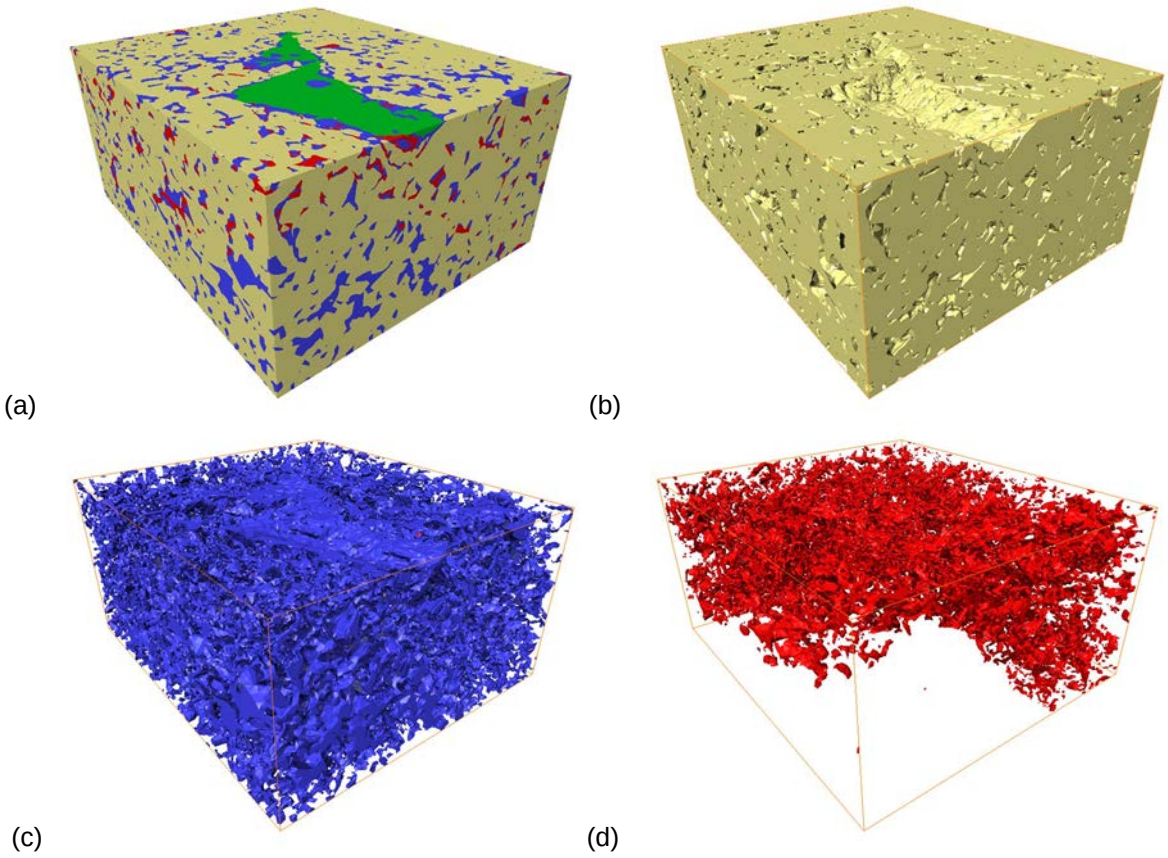

Figure 7. 3D reconstructed image describing corrosion damage – microstructure interaction for the hardmetal studied (after 168h of exposure time) at both global and individual phase levels: (a) global scenario (including surface microcrater in green); (b) WC skeleton in yellow; (c) metallic binder in blue, and (d) corrosion-induced microcracks in red.

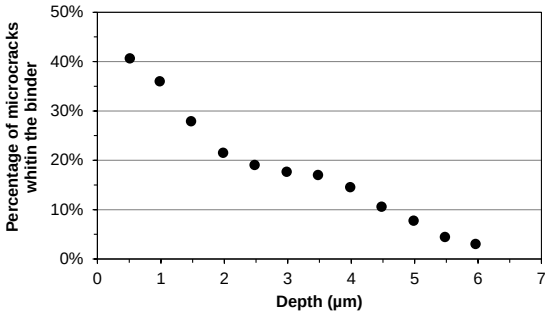

Figure 8. Relative amount of microcracks (resulting from corrosion within binder) as a function of depth from surface (exposure time: 168h).

Regarding description of the corrosion scenario discerned in this investigation, it seems clear that binder and microcrack “phases” are relevant features for describing damage-microstructure interaction in the hardmetal studied. Within this context, the contiguity (networking) character and relative distribution of each of those phases becomekey parameters for assessing its effective detrimental effects on properties, such as fracture strength. In this study, characterization of these parameters is attempted by means of *skeletonization*, an image analysis technique that consists in transforming a phase of interest in filaments whose diameter and colour are related to its local size. Hence, as the volume occupied at small length scale by the phase under consideration increases, corresponding cord diameter gets higher and more intensely red. On the opposite side, if presence of the phase at the “bulk” level becomes scarcer, filaments become thinner and more intensely blue. Skeletonization of binder and corrosion-induced microcrack reconstructed phases are shown in **Figure 9**. It may be highlighted that interconnecting nature for each “phases network” is different: long range / fully interconnected for the binder case, and short range / locally interconnected for the damage one.

The fact that lower contiguity is discerned within the microcrack network as subsurface level under consideration becomes deeper is in complete concordance with the 3D description detailed above.

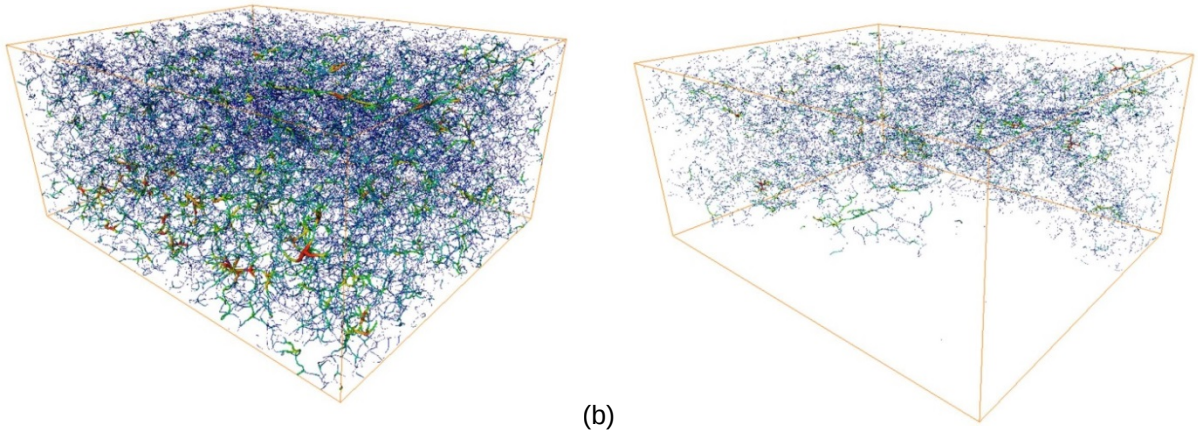

(a) (b)

Figure 9. Skeletonization corresponding to; (a) binder and (b) microcracked phases.

4. Summary and concluding remarks

In this work the damage induced by corrosion in a WC-Co hardmetal is investigated. Samples were immersed in an agitated mine water solution for different times and tolerance to corrosion damage was evaluated by measuring the retained strength of corroded specimens. Results show that corrosion damage results in relevant strength degradation. Extensive fractographic inspection permitted to rationalize the detrimental influence on the basis of stress raising effects associated with localized and heterogeneous metal binder dissolution – corrosion pits - at the corrosion front level. A detailed characterization of corrosion-induced damage through 3D FIB-FESEM tomography provides further support to above ideas: localized corrosion pits with variable and partial interconnectivity (as a function of depth), and evolution from microcracknucleation associated with binder dissolution to pronounced binder removal,which finally leaves an effectively unbound WC skeleton behind it. However, as corrosion damage evolves, it gets homogenized because stress concentration effects associated with localized pits get geometrically lessened. As a consequence, relative changes in residual strength become less pronounced with increasing exposure time.

AWKNOLEDGEMENTS

This work was financially supported by the Spanish Ministerio de Economía y Competitividad (Grant MAT2012-34602). The support received from Direcció General de Recerca del Comissionat per a Universitats i Recerca de la Generalitat de Catalunya through recognition of CIEFMA as Grup de Recerca Consolidat 2014SGR130is also acknowledged. Additionally, J.M. Tarragó and Joan Josep Roa would like to acknowledge financial support received from the collaborative Industry-University program between Sandvik Hyperion and Universitat Politècnica de Catalunya (PhD scholarship) and the Juan de la Cierva Programme, respectively.

BIBLIOGRAPHY

[1] Pugsley VA, Korn G, Luyckx S, Sockel HG, Heinrich W, Wolf M, et al. The influence of a corrosive wood-cutting environment on the mechanical properties of hardmetal tools. Int J Refract Met Hard Mater 2001;19:311–8.

[2] Beste U, Hartzell T, Engqvist H, Axén N. Surface damage on cemented carbide rock-drill buttons. Wear 2001;249:324–9.

[3] Beste U, Coronel E, Jacobson S. Wear induced material modifications of cemented carbide rock drill buttons. Int J Refract Met Hard Mater 2006;24:168–76.

[4] Lu R, Minarro L, Su Y-Y, Shemenski RM. Failure mechanism of cemented tungsten carbide dies in wet drawing process of steel cord filament. Int J Refract Met Hard Mater 2008;26:589–600.

[5] Konyashin I. Cemented Carbides for Mining, Construction and Wear Parts. In: Sarin VK, Mari D, Llanes L, editors. Comprehensive Hard Materials, Elsevier; 2014, Chapter 1.15, Volume 1, p. 425-51.

[6] Tomlinson WJ, Linzell CR. Anodic polarization and corrosion of cemented carbides with cobalt and nickel binders. J Mater Sci 1988;23:914–8.

[7] Tomlinson WJ, Ayerst N. Anodic polarization and corrosion of WC-Co hardmetals containing small amounts of Cr_3C_2 and/or VC. J Mater Sci 1989; 24: 2348–54.

[8] Scholl H, Hofman B, Rauscher A. Anodic polarization of cemented carbides of the type [(WC,M): M = Fe, Ni or Co] in sulphuric acid solution. Electrochim Acta 1992;37:447–52.

[9] Human AM, Exner HE. Electrochemical behavior of tungsten-carbide hardmetals. Mater Sci Eng A 1996; 209: 180–91.

[10] Upadhyaya GS. Cemented tungsten carbides: production, properties, and testing. New Jersey, USA: Noyes Publications; 1998.

[11] Sutthiruangwong S, Mori G. Corrosion properties of Co-based cemented carbides in acidic solutions. Int J Refract Met Hard Mater 2003;21:135–45.

[12] Pugsley VA, Sockel H-G. Corrosion fatigue of cemented carbide cutting tool materials. Mater Sci Eng A 2004;366:87–95.

[13] Schnyder B, Stössel-Sittig C, Rüdiger K, Hochstrasser-Kurz S, Virtanen S, Jaeggi C, Eichenberger N, Siegenthaler H. Investigation of the electrochemical behaviour of WC-Co hardmetal with electrochemical and surface analytical methods. Surf Sci 2004; 566-568: 1240-45.

[14] Sutthiruangwong S, Mori G, Kösters R. Passivity and pseudopassivity of cemented carbides. Int J Refract Met Hard Mater 2005;23:129–36.

[15] Barbatti CF, Sket F, Garcia J, Pyzalla A. Influence of binder metal and surface treatment on the corrosion resistance of (W,Ti)C-based hardmetals. Surf Coat Technol 2006; 201: 3314-27.

[16] Hochstrasser(-Kurz) S, Mueller Y, Latkoczy C, Virtanen S, Schmutz P. Analytical characterization of the corrosion mechanisms of WC-Co by electrochemical methods and inductively coupled plasma mass spectroscopy. Corros Sci 2007; 49: 2002-20.

[17] Bozzini B, Busson B, De Gaudenzi GP, D'Urzo L, Mele C, Tadjeddine A. An SFG and ERS investigation of the corrosion of $CoW_{0.013}C_{0.001}$ alloys and WC-Co cermets in CN^-containing aqueous solutions. Corros Sci 2007; 49: 2392-405.

[18] Kellner FJJ, Hildebrand H, Virtanen S. Effect of WC grain size on the corrosion behavior of WC–Co based hardmetals in alkaline solutions. Int J Refract Met Hard Mater 2009; 27: 806-12.

[19] Potgieter JH, Thanjekwayo N, Olubambi P, Maledi N, Potgieter-Vermaak SS. Influence of Ru additions on the corrosion behaviour of WC–Co cemented carbide alloys in sulphuric acid. Int J Refract Met Hard Mater 2011; 29: 478-87.

[20] Gant AJ, Gee MG, May AT. The evaluation of tribo-corrosion synergy for WC–Co hardmetals in low stress abrasion. Wear 2004; 256: 500-16.

[21] Thakare MR, Wharton JA, Wood RKJ, Menger C. Exposure effects of alkaline drilling fluid on the microscale abrasion–corrosion of WC-based hardmetals. Wear 2007; 263: 125-36.

[22] Gant AJ, Gee MG, Gohil DD, Jones HG, Orkney LP. Use of FIB/SEM to assess the tribo-corrosion of WC/Co hardmetals in model single point abrasion experiments. Tribol Int 2013;68:56–66.

[23] Cairney JM, Munroe PR, Schneibel JH. Examination of fracture surfaces using focused ion beam milling. Acta Metall 2000;42:473–8.

[24] Mingard KP, Jones HG, Gee MG, Roebuck B, Gholinia A, Winiarski B, et al. 3D Imaging of structures in bulk and surface modified WC-Co hardmetals. Proceedings EuroPM2012, Basel: EPMA; 2012, p. 155–60.

[25] Tarragó JM, Jiménez-Piqué E, Turón M, Rivero L, Schneider L, Llanes L. Toughening and fatigue micromechanisms in hardmetals: FESEM/FIB tomography characterization. In: Sigl LS, Kestler H, Wagner J, editors. Proc. 18th Plansee Seminar, Reutte, Austria: Plansee SE; 2013 [HM54/1-9]

[26] Roebuck B, Almond EA. Deformation and fracture processes and the physical metallurgy of WC–Co hardmetals. Int Mater Rev 1988;33:90–110.

[27] Torres Y. Comportamiento a fractura y fatiga de carburos cementados WC–Co. PhD Thesis Universitat Politècnica de Catalunya; 2002.

[28] Coureaux D. Comportamiento mecánico de carburos cementados WC–Co: Influencia de la microestructura en la resistencia a la fractura, la sensibilidad a la fatiga y la tolerancia al daño inducido bajo solicitaciones de contacto. PhD Thesis Universitat Politècnica de Catalunya; 2012.

[29] Torres Y, Casellas D, Anglada M, Llanes L. Fracture toughness evaluation of hardmetals: influence of testing procedure. Int J Refract Met Hard Mater 2001;19:27–34.

[30] Allen C. Corrosion of galvanized steel in synthetic mine water. Br Corros J 1991;26;93-102.